Light-Induced Reduction of Bovine Adrenodoxin via the Covalently Bound Ruthenium(II) Bipyridyl Complex: Intramolecular Electron Transfer and Crystal Structure†

Andrei Halavaty,‡ Jürgen J. Müller,‡ Jörg Contzen,§ Christiane Jung,§ Frank Hannemann,|| Rita Bernhardt,|| Marcus Galander,⊥ Friedhelm Lendzian,⊥ and Udo Heinemann*,‡,#

Crystallography Group and Protein Dynamics, Max-Delbrück-Centrum für Molekulare Medizin, Robert-Rössle-Strasse 10, D-13125 Berlin-Buch, Germany, Department of Biochemistry, Universität des Saarlandes, Postfach 15 11 50, D-66041 Saarbrücken, Germany, Max-Volmer-Laboratorium für Biophysikalische Chemie, Institut für Chemie, Technische Universität Berlin, PC 14, Strasse des 17. Juni 135, D-10623 Berlin, Germany, and Institut für Chemie/Kristallographie, Freie Universität, Takustrasse 6, D-14195 Berlin, Germany

Received June 1, 2005; Revised Manuscript Received November 18, 2005

ABSTRACT: Bovine adrenodoxin (Adx) plays an important role in the electron-transfer process in the mitochondrial steroid hydroxylase system of the bovine adrenal cortex. Using electron paramagnetic resonance (EPR) spectroscopy, we showed that photoreduction of the [2Fe-2S] cluster of Adx via (4′-methyl-2,2′-bipyridine)bis(2,2′-bipyridine)ruthenium(II) [$Ru(bpy)_2(mbpy)$] covalently attached to the protein surface can be used as a new approach to probe the "shuttle" hypothesis for the electron transfer by Adx. The 1.5 Å resolution crystal structure of a 1:1 $Ru(bpy)_2(mbpy)$−Adx(1−108) complex reveals the site of modification, Cys95, and allows to predict the possible intramolecular electron-transfer pathways within the complex. Photoreduction of uncoupled Adx, mutant Adx(1−108), and $Ru(bpy)_2(mbpy)$−Adx(1−108) using safranin T as the mediating electron donor suggests that two electrons are transferred from the dye to Adx. The intramolecular photoreduction rate constant for the ruthenated Adx has been determined and is discussed according to the predicted pathways.

The mechanism of transfer of six electrons from the reduced nicotinamide adenine dinucleotide phosphate (NADPH)[1] to the terminal heme protein, side-chain-cleavage cytochrome P450 ($P450_{scc}$), via a membrane-attached flavoprotein, adrenodoxin reductase (AR), and an electron-transferring non-heme iron protein, Adx, has not been finally explored. Three alternative models have been suggested in the literature: (i) a "shuttle" model in which Adx carries electrons from AR to $P450_{scc}$ by sequential binding to these proteins (*1*, *2*), (ii) an electron transfer through an organized ternary complex of AR, Adx, and $P450_{scc}$ (*3*), and (iii) a quaternary complex of AR, Adx dimer, and $P450_{scc}$ (*4*).

On the basis of our previous crystallographic (*5*, *6*) and cross-linking (*7*, *8*) as well as nuclear magnetic resonance (NMR) (*8*) results, we are in favor of the shuttle hypothesis. This model is supported by the lack of activity of the cross-linked Adx−$P450_{scc}$ complex within the reconstituted steroid hydroxylase system and the observation of largely overlapping Adx surface areas involved in interactions with both AR and $P450_{scc}$. To probe the "shuttle model", we used a photosensitive ruthenium complex to examine whether a single Adx could be reduced in the absence of AR.

In this study, we report the preparation of the ruthenium complex-modified bovine Adx, its crystal structure, and its susceptibility to photoreduction. On the basis of the high-resolution crystal structure of the modified Adx, possible intramolecular electron-transfer pathways are proposed.

MATERIALS AND METHODS

Construction of pET3d-AdxZNT108. The plasmid pKKAdx (*9*) was used as a template in order to amplify the Adx

† This work was supported by the DFG, Projects He 1318/19-3.4 and Ju 229/4-3.

* To whom correspondence should be addressed at the Crystallography Group, Max-Delbrück-Centrum für Molekulare Medizin. Phone: (49 30) 94063420. Fax: (49 30) 94062548. E-mail: heinemann@mdc-berlin.de.

‡ Crystallography Group, Max-Delbrück-Centrum für Molekulare Medizin.

§ Protein Dynamics, Max-Delbrück-Centrum für Molekulare Medizin.

|| Universität des Saarlandes.

⊥ Technische Universität Berlin.

Freie Universität.

[1] Abbreviations: Adx, adrenodoxin; Adx(C95S), adrenodoxin mutant with cysteine-to-serine substitution; Adx(1−108) and Adx(4−108), truncated forms of Adx; AR, adrenodoxin reductase; CO, carbon monoxide; DMSO, dimethyl sulfoxide; DTT, 1,4-dithiothreitol; EDTA, ethylenediaminetetraacetic acid; EPR, electron paramagnetic resonance; ES-TOF-MS, electrospray time-of-flight mass spectrometry; FPLC, fast protein liquid chromatography; IPTG, isopropyl β-D-thiogalactopyranoside; MLCT, metal-to-ligand charge transfer; N-6×His tag, N-terminal 6×His tag; NADPH, reduced nicotinamide adenine dinucleotide phosphate; $Na_2S_2O_4$, sodium dithionite; NMR, nuclear magnetic resonance; $P450_{cam}$, camphor monooxygenase from *Pseudomonas putida*; $P450_{scc}$, side-chain cleavage cytochrome P450; PDB, Protein Data Bank; PCR, polymerase chain reaction; rmsd, root-mean-square deviation; $Ru(bpy)_2(Br\text{-}mbpy)(PF_6)_2$, (4-bromomethyl-4′-methyl-2,2′-bipyridine)bis(2,2′-bipyridine)ruthenium(II) bishexafluorophosphate; $Ru(bpy)_2(mbpy)$−Adx(1−108), $Ru(bpy)_2(mbpy)$-modified Adx(1−108); Ru(II)*, excited state of the ruthenium complex; SDS−PAGE, polyacrylamide gel electrophoresis with sodium dodecyl sulfate; $Ru(bpy)_3$, tris(2,2′-bipyridyl)dichlororuthenium(II) hexahydrate; Xa, factor Xa.

10.1021/bi0510330 CCC: $33.50
Published on Web 12/22/2005

fragment with the N-terminal 6×His tag (N-6×His tag) using 5′-ACT GCC ATG GGT CAC CAC CAC CAC CAC CAC ATC GAA GGT CGA-3′ and 5′-GGG GAA GCT TAT TCT ATC TTT GAG TTC-3′ primers. The PCR fragment encoding the N-6×His tag followed by the factor Xa (Xa) cleavage site and the sequence of 128 amino acids of bovine Adx was ligated into the expression vector pET3d (*10*) after the *Nco*I/*Bam*HI restriction. A stop codon was inserted following the sequence, encoding 108 amino acid residues of Adx (pET3d-AdxZNT108). Site-directed mutagenesis was performed with the mutagenic primers 5′-ACT GTT CGA GTA CCT TAA GCC GTG TCT GAT GCC-3′ and 5′-GGC ATC AGA CAC GGC TTA AGG TAC TCG AAC AGT-3′ using the QuikChange mutagenesis protocol (Stratagene Ltd., Cambridge, U.K.).

Proteins. BL21(DE3)pLysE CodonPlus (Novagen, Darmstadt, Germany) with pET3d-AdxZNT108 was cultivated in Luria−Bertani medium with ampicillin (100 μg/mL) and chloramphenicol (50 μg/mL) overnight at 37 °C. Adx was overexpressed by adding 1 mM isopropyl β-D-thiogalactopyranoside (IPTG) at 30 °C for 12 h. Cells were harvested at 4 °C by centrifugation at 8000 rpm for 10 min and stored at −70 °C. The thawed *Escherichia coli* cells were disrupted in a French Press (Spectronic Unicam) in 20 mM Tris-HCl buffer, pH 7.4 (buffer A), containing 300 mM KCl and 10 mM imidazole. Adx was purified on Ni-NTA agarose (Qiagen GmbH, Hilden, Germany) using 250 mM imidazole in buffer A. Further, using DEAE 52 cellulose Servacel (Serva Electrophoresis GmbH, Heidelberg, Germany) the mutant protein was eluted over a linear gradient (0−50%) of 1 M KCl in buffer A. Adx homogeneity was analyzed by a fast protein liquid chromatography (FPLC) on the HiLoad 26/60 Superdex 200 (Amersham Pharmacia Biotech, Freiburg, Germany).

Expression and purification of the Adx mutant with cysteine-to-serine substitution [Adx(C95S)] was described elsewhere (*9*). Recombinant Adx and AR were expressed and purified as described (*11*), and $P450_{scc}$ was isolated and purified from the mitochondria of bovine adrenal cortex (*12*). The purity of Adx, AR, and $P450_{scc}$ was estimated with A_{414}/A_{276}, A_{280}/A_{450}, and A_{393}/A_{276} ratios, respectively. The concentrations were determined using $\epsilon_{414} = 9.8$ (mM cm)$^{-1}$ (*13*) and $\epsilon_{450} = 10.9$ (mM cm)$^{-1}$ (*14*) for Adx and AR, respectively. The $P450_{scc}$ concentration was determined using the carbon monoxide (CO) difference spectrum, assuming $\epsilon_{450-490} = 91$ (mM cm)$^{-1}$ (*15*). All UV−vis spectra were obtained on the UV−vis scanning spectrophotometer UV-2102 (Shimadzu, Kyoto, Japan).

Enzymatic Cleavage of the N-6×His Tag and Purification of Adx(1−108). A protocol for the Novagen factor Xa cleavage capture kit (Calbiochem-Novabiochem GmbH, Schwalbach/Ts., Germany) was used with slight modifications. For enzymatic cleavage of the fusion 6×His tag a frozen stock solution of Adx(N-6×His tag/Xa/1−108) or the protein after gel filtration was used. Adrenodoxin was first concentrated to a final volume of ≤0.5 mL and final concentration of ≤0.001 M in 0.05 M Tris-HCl, pH 8.0, 0.1 M NaCl, and 0.005 M $CaCl_2$. The reaction was carried out with a 20:1 (Adx:Xa) molar ratio at 4 °C for 20 h to prevent possible protein degradation at room temperature. After incubation time Xa was inhibited with 0.001 M Pefablock SC (Pentapharm Ltd., Basel, Switzerland) at room temperature (15 min) before the reaction mixture was applied to the affinity capture Xarrest agarose. Then, the sample was loaded, gently mixed with the agarose, and incubated for 5 min to increase the binding of Xa. Adrenodoxin was recovered by spin filtration at room temperature at 2000 rpm for 5 min. Collected protein was applied to a small Ni-NTA test column to check the completeness of the reaction. The protein homogeneity after cleavage of the N-6×His tag was analyzed by FPLC, 18% polyacrylamide gel electrophoresis with sodium dodecyl sulfate (SDS−PAGE), and electrospray time-of-flight mass spectrometry (ES-TOF-MS).

Covalent Modification of Adx(1−108). Solid (4-bromomethyl-4′-methyl-2,2′-bipyridine)bis(2,2′-bipyridine)ruthenium(II) bishexafluorophosphate [$Ru(bpy)_2$(Br-mbpy)$(PF_6)_2$] was used for modification of Adx(1−108) as described for camphor monooxygenase from *Pseudomonas putida* ($P450_{cam}$) (*16*). Stereoselective purification of the ruthenium complex was not carried out. Adrenodoxin was concentrated to a final volume of 0.5 mL and concentration of ≤0.001 M in 0.1 M potassium phosphate buffer, pH 8.0, and then preincubated (4 °C, 30 min) with a 3-fold molar excess of 1,4-dithiothreitol (DTT) (Carl Roth GmbH & Co. KG, Karlsruhe, Germany) to avoid formation of disulfide bonds. A tenfold molar excess of $Ru(bpy)_2$(Br-mbpy)$(PF6)_2$ was dissolved in dimethyl sulfoxide (DMSO) (Merck KGaA, Darmstadt, Germany) and added to an aliquot of the protein, and then the reaction mixture was incubated with slight shaking for 2 h in the dark. The reaction was stopped by removing the excess of reagents on Sephadex G-25 M (Amersham Pharmacia Biotech, Freiburg, Germany), preequilibrated with 0.05 M Tris-HCl buffer, pH 7.4, at 4 °C. The crude reaction mixture was further purified over a (0−50%) gradient of 1 M KCl in buffer A on a Bioscale Q2 column using the BioLogic high-pressure chromatography system (Bio-Rad Laboratories, Inc., München, Germany). The stoichiometry of $Ru(bpy)_2$(mbpy) bound to Adx(1−108) was determined as described (*16*). To prove that Cys95 is the modification site, the Adx(C95S) mutant was labeled with the ruthenium complex and further purified as described for Adx(1−108).

Mass Spectrometry. The electrospray time-of-flight mass spectrometry (ES-TOF-MS) was performed to check the molecular weights of Adx(1−108) and $Ru(bpy)_2$(mbpy)−Adx(1−108). Mass spectra were obtained employing a Q-TOF1 mass spectrometer (Micromass, Manchester, U.K.) with an accuracy of 0.01%. The protein solutions were desalted on Poros R1 material (Applied Biosystems, Darmstadt, Germany), eluted with 60% acetonitrile, 39% water, and 1% formic acid, and introduced via a Harvard syringe pump at a flow rate of 200 nL/min.

Redox Potential Measurements. Redox potentials of Adx, Adx(1−108), and $Ru(bpy)_2$(mbpy)−Adx(1−108) were determined using the dye photoreduction method with safranin T (Sigma-Aldrich, Steinheim, Germany) as an indicator and mediator (*17*). In the presence of ethylenediaminetetraacetic acid (EDTA) the oxidized dye can be converted to its colorless reduced form by illumination. $P450_{cam}$ was used as a reference protein for a typical one-electron acceptor instead of $P450_{scc}$, because the latter has been less investigated. The reaction conditions (2.6 mL) for each protein were 0.1 M potassium phosphate buffer, pH 7.3, containing 0.01 M EDTA (Carl Roth GmbH & Co. KG, Karlsruhe, Germany), freshly prepared glucose (8 mg/mL), 18 μL of 0.001

M safranin T, and the oxygen scavenger system (4 mg/mL glucose oxidase and 2 mg/mL catalase). First, a protein solution was stirred with N_2 for 30 min in a black precision cell of quartz (Hellma GmbH & Co., KG, Müllheim, Germany) and finally incubated with the oxygen scavenger system in the dark for the next 30 min. All oxidized and reduced spectra were obtained anaerobically. Reduction was initiated by illumination steps (3−5 s) of the sample with a 500 W xenon lamp. After each illumination step, the spectrum (320−700 nm) was immediately recorded. A total of 10−15 illuminations were carried out. The redox potentials were determined using the Nernst equation (eq 1) under equilibrium conditions, where the potentials of the dye and the protein are equal ($E_{dye} = E_{protein}$):

$$E_{0(dye)} + 2.303\frac{RT}{n_{dye}F}\log\frac{[C_{ox(dye)}]}{[C_{red(dye)}]} = E_{0(protein)} + 2.303\frac{RT}{n_{protein}F}\log\frac{[C_{ox(protein)}]}{[C_{red(protein)}]} \quad (1)$$

where R, T, F, $n_{protein}$, and n_{dye} are the gas constant, temperature (K), the Faraday constant, and the number of electrons transferred in the reaction for each redox pair of the protein (Adx or P450$_{cam}$) and the dye, respectively. $E_{0(dye)}$ and $E_{0(protein)}$ are the standard redox potentials given in millivolts. [C_{ox}] and [C_{red}] represent the concentrations of the oxidized and reduced components, respectively. The ratio [C_{ox}]/[C_{red}] was determined as $(1 - a)/a$, where a represents the fraction of the reduced component. The a is determined from the ratio of the absorbance change in the difference spectrum (spectrum after illumination minus spectrum without illumination) at 414 nm (for Adx) and at 521 nm (for safranin T) to the maximal absorbance change produced for 100% reduction, which was induced by sodium dithionite addition at the end of the experiments. In a separate experiment, it was found that dithionite is able to completely reduce Adx as well as the dye, which is the prerequisite to apply this procedure. Using $n_{dye} = 2$ and an $E_{0(dye)}$ of −289 mV for safranin T (*18*), the redox potential for each illumination step was determined using the left side of eq 1. These potentials were then plotted versus the decadic logarithm of [$C_{ox(protein)}$]/[$C_{red(protein)}$]. From the slope and y intercept of the linear fit of the experimental points, the number of transferred electrons, $n_{protein}$, and the standard redox potential $E_{0(protein)}$, respectively, for Adx and P450$_{cam}$ were determined.

Electron-Transfer Capability of Adrenodoxin. Adx, Adx(1−108), and Ru(bpy)$_2$(mbpy)−Adx(1−108) were investigated using the cytochrome *c* reduction (*11*) and NADPH-induced reduction of P450$_{scc}$ assays (*19*). The kinetics of the cytochrome *c* reduction was investigated in 0.033 M potassium phosphate buffer, pH 7.4, at room temperature. The reaction mixture (1 mL) contained 60 μM cytochrome *c* (Boehringer Mannheim GmbH, Germany), 2 μM AR, and variable amounts (0.05−1.5 μM) of the investigated adrenodoxins. The reaction was started by adding NADPH at a final concentration of 0.14 mM. Reduction of cytochrome *c* was monitored by measurement of the increase of the absorbance at 550 nm. The activities were calculated using $\epsilon_{550} = 20$ (mM cm)$^{-1}$ for the reduced minus oxidized cytochrome *c* (*11*).

Enzymatic reduction of P450$_{scc}$ was studied in the reconstituted steroid hydroxylase system in 0.033 M potassium phosphate buffer, pH 7.4, at room temperature. The reaction mixture (1 mL) containing 0.67 μM P450$_{scc}$, 3.34 nM AR, and 0.33−1.67 μM Ru(bpy)$_2$(mbpy)−Adx(1−108) was treated with CO for 2 min, avoiding foam formation in the sample. Samples with Adx (0.33−1.67 μM) and unmodified Adx(1−108) (0.33−1.67 μM) were prepared in the same manner as ruthenated Adx(1−108). After saturation with CO the reaction in all samples was initiated by adding the NADPH-regenerating system [0.14 mM NADPH, 0.002 M glucose 6-phosphate, and 1 unit/mL glucose-6-phosphate dehydrogenase (all from Serva Feinbiochemica GmbH & Co., KG, Heidelberg, Germany)]. Formation of the CO−heme complex was detected by an appearance of the peak at 450 nm.

Photoreduction of Adx(1−108). The applicability of the photoreduction method was checked first with unmodified Adx(1−108) in buffer A containing 0.1 M EDTA and 10% glycerol to see whether the protein stability might be affected by irradiation. The sample (0.1 mL) was gently stirred with nitrogen for 1 h before illumination in a black precision cell of quartz with a small optical window (2 mm × 2 mm). The sample was then irradiated for 60 min (in 10 min intervals) at 25 °C using the argon ion laser Innova 90 (Coherent, Inc., Palo Alto, CA) at 457.9 nm with the final output of 60 mW. The stability was checked spectrophotometrically. The 1:1 Ru(bpy)$_2$(mbpy):Adx(1−108) sample was prepared in the same manner and exposed for 20−40 min in an EPR tube and 75 min for spectroscopic studies. Photoreduction was monitored by the decrease of the absorbance at 414 nm. Reoxidation was done at 4 °C. EDTA has been used as a sacrificial electron donor that reacts irreversibly with Ru^{3+} to form Ru^{2+}. The rate of EDTA oxidation is $k_Q = 1.1 \times 10^8$ M^{-1} s^{-1} (*20*). The usage of 0.1 M EDTA ensures that all Ru^{3+} formed during illumination are instantaneously reduced to Ru^{2+}, thus minimizing the Fe^{2+}/Ru^{3+} back-transfer, and that the EDTA concentration can be assumed as constant during the experiment. Addition of 0.1 M EDTA to the samples had no influence on the spectrum of the Ru(bpy)$_2$(mbpy)−Adx(1−108) complex.

The observed reduction rates (k_{obs}) were derived from the slope of the plot ln(1 − α) versus illumination time t (*16*), where α is the fraction of the photoreduced Adx(1−108). Rates k_{et} at three different Ru(bpy)$_2$(mbpy)−Adx(1−108) concentrations (0.01, 0.05, and 0.17 mM) were calculated using eq 2 according to Contzen et al. (*16*):

$$k_{et} = \frac{k_d}{(I_0\kappa d/k_{obs}) - 1} \quad (2)$$

where k_d summarizes all decay processes of the excited ruthenium complex (*16*). Its value of $(7 \pm 1) \times 10^6$ s^{-1} was determined for Ru(bpy)$_3$−cytochrome *c* (*21*, *22*) and assumed to be also an approximate value for the ruthenium complex used here. I_0, κ, and d are the intensity of the laser, extinction coefficient of the ruthenium complex absorption at 457.9 nm, and optical path length, respectively. The error of k_{et} is calculated taking into account the errors arising from fluctuations of the illuminating laser power (±0.5%) and the errors of k_d, and k_{obs} as described (*16*). The rate constant k_{et} consists of two contributions (eq 3). The intermolecular (k_{et2})

rate constant was determined from the slope in the plot k_{et} versus the concentrations of Ru(bpy)$_2$(mbpy)−Adx(1−108). The intramolecular rate (k_{et1}) is obtained from the extrapolation of the Ru(bpy)$_2$(mbpy)−Adx(1−108) concentration to zero using the equation:

$$k_{et} = k_{et1} + k_{et2}[\text{Ru(bpy)}_2\text{(mbpy)} - \text{Adx(1−108)}] \quad (3)$$

EPR. "Negative" control samples [Adx(1−108), water-soluble tris(2,2′-bipyridyl)dichlororuthenium(II) hexahydrate (Ru(bpy)$_3$) (Sigma-Aldrich, Steinheim, Germany) plus Adx(1−108) in a 1:1 ratio, and just the water-soluble ruthenium complex itself] and Ru(bpy)$_2$(mbpy)−Adx(1−108) were thoroughly deoxygenated with nitrogen for 1 h as described (*23*). Then, each EPR sample tube was placed in the laser beam, so that the tube length and laser beam were aligned in parallel. This ensures an optimal irradiation of the samples. Additionally, the sample with Adx(1−108) ("positive" control) was reduced in an EPR tube with fresh solid sodium dithionite ($Na_2S_2O_4$). After illumination and chemical reduction, the samples were flash-frozen by immersing the EPR tubes into liquid nitrogen. EPR measurements were performed on an X-band (9.5 GHz) EPR spectrometer (Bruker 300E, Germany) equipped with an Oxford ESR 9 helium flow cryostat at 80 K with modulation frequency, 12.5 kHz; microwave power, 5 mW; and modulation amplitude, 5 G [10 G for the illuminated sample of Ru(bpy)$_2$(mbpy)−Adx(1−108)]. The spin quantification of the reduced [2Fe-2S] cluster of Adx(1−108) was carried out using $CuSO_4$ as a standard (*24*).

Crystallization of Ru(bpy)$_2$(mbpy)−Adx(1−108). The modified protein was crystallized by the hanging-drop vapor diffusion method as described for Adx(4−108) (*5*). Crystals grew in 1 week at 4 °C. Data were collected at 90 K on a MAR-165CCD at X06SA-PX (Swiss Light Source, Villigen, Switzerland). Processing, scaling, and conversion were done with XDS (*25*).

Structure Determination and Refinement. An initial structure of the 1:1 Ru(bpy)$_2$(mbpy):Adx(1−108) complex was determined by molecular replacement using AMoRe (*26*) and Adx(4−108) (*5*) [Protein Data Bank (PDB) entry 1AYF] as a search model. The structure was refined with REFMAC (*27*) at 20−1.5 Å resolution including (i) isotropic refinement of Adx(1−108) without the ruthenium complex, (ii) placement of water molecules, and (iii) positioning of the ruthenium moiety into the remaining difference density and subsequent refinement. The coordinates of the ruthenium complex isomers were adapted from the PDB entry 1K2O (*28*). Refinement results and fitting of the ruthenium complex were analyzed using the graphical display program O (*29*). Grouped TLS refinement produced the final model. The density of the ruthenium moiety and side chain of Cys95 was improved using the program EDEN (*30*). Possible electron-transfer pathways within the Ru(bpy)$_2$(mbpy)−Adx(1−108) complex were calculated using the program HARLEM (*31*). The two crystal structures, Ru(bpy)$_2$(mbpy)−Adx(1−108) and unmodified Adx(4−108) (1AYF), were compared by least-squares fitting of their C$^\alpha$ positions using the program LSQKAB (*32*).

RESULTS

1:1 Ru(bpy)$_2$(mbpy):Adx(1−108) Complex. The complex was eluted from a Bioscale Q2 column at 23−24% of 1 M KCl in buffer A. Differences in the visible spectra of the oxidized Adx(1−108) and the modified Adx(1−108) are due to the spectral contribution of the ruthenium complex in the spectrum of Adx(1−108) (Figure 1). Adx, Adx(1−108), and Ru(bpy)$_2$(mbpy)−Adx(1−108) were active in transporting electrons to cytochrome *c* and P450$_{scc}$ (Table 1 and Figure 2). No specific 1:1 covalent complex of Adx(C95S) with the ruthenium complex could be purified.

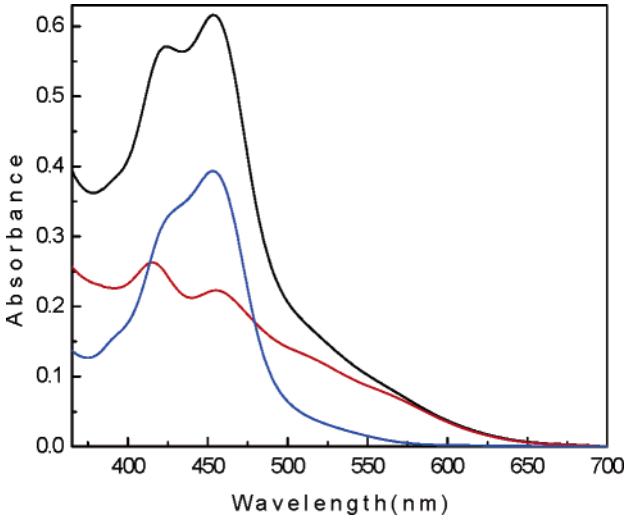

FIGURE 1: Modification of Adx(1−108) with Ru(bpy)$_2$(mbpy). The absorption spectra are Ru(bpy)$_2$(mbpy)-free Adx(1−108) (0.026 mM; red), free ruthenium complex (0.026 mM; blue), and 1:1 Ru(bpy)$_2$(mbpy)−Adx(1−108) complex (black).

Table 1: Cytochrome *c* Reduction Assay

protein	activity [nmol min^{-1} (nmol of Adx)$^{-1}$][a]
Adx	59.5 ± 3.2[b]
Adx(1−108)	62.5 ± 7.0
Ru(bpy)$_2$(mbpy)−Adx(1−108)	40.2 ± 4.0

[a] Cytochrome *c* reduction was followed at 550 nm in the presence of 0.14 mM NADPH. [b] Standard deviations were calculated from two independent experiments, including six measurements with variable concentrations of substrates.

Mass Spectrometry Data. Data revealed complete cleavage of the N-6×His tag and formation of the 1:1 Ru(bpy)$_2$(mbpy):Adx(1−108) complex. Experimental molecular masses of 11879.0 Da [Adx(1−108)] and 12470.5 Da [Ru(bpy)$_2$(mbpy)−Adx(1−108)] correspond to the theoretical values, 11880.4 and 12472.04 Da, respectively, calculated without the [2Fe-2S] cluster.

Crystal Structure of 1:1 Ru(bpy)$_2$(mbpy):Adx(1−108). The structure is deposited with the PDB under the access code 2BT6. Crystallographic data are summarized in Table 2. Generally, molecule A of the Ru(bpy)$_2$(mbpy)−Adx(1−108) complex was better refined than molecule B in the asymmetric unit.

Prominent electron density, which protrudes from the protein surface in the form of open circles, indicating the presence of aromatic rings, was observed in the vicinity of Cys95 of both Adx(1−108) molecules in the asymmetric unit. Positioning of one of the two Ru(bpy)$_2$(mbpy) isomers into this density and subsequent refinement confirmed the presence of the ruthenium complex in the crystal structure. Clearly observed $2F_o - F_c$ electron density between the C^{39} atom of the Ru(bpy)$_2$(mbpy) moiety and the side chain of

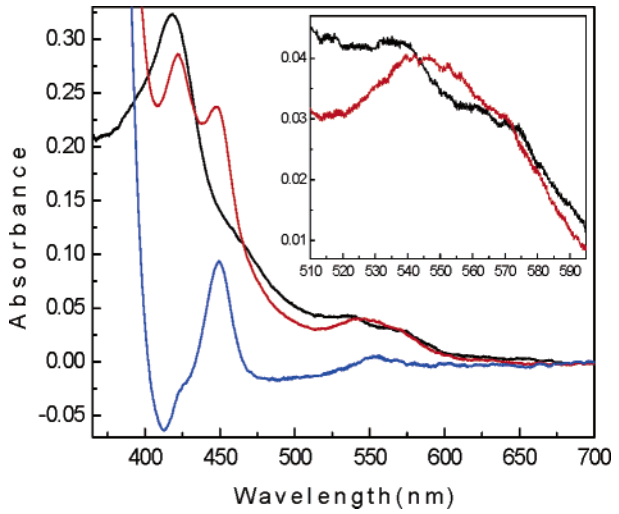

FIGURE 2: NADPH-induced reduction of P450$_{scc}$. Oxidized (black) spectrum and carbon monoxide-bound form (red) spectrum of reduced P450$_{scc}$ (0.67 μM) when the 1:1 Ru(bpy)$_2$(mbpy)−Adx(1−108) complex was used as an electron carrier in the reconstituted steroid hydroxylase system [for Adx and Adx(1−108) data are not shown]. CO-difference spectrum of P450$_{scc}$ (blue). (Inset) Close-up view of the oxidized and CO-treated after reduction spectra of P450$_{scc}$. Concentrations of all three adrenodoxins were in the range between 0.33 and 1.67 μM.

Cys95 confirms the existence of the covalent link. Residual difference density revealed the simultaneous binding to Adx(1−108) of the other Ru(bpy)$_2$(mbpy) isomer in the crystal lattice. The side-chain conformation of Cys95 differs, depending on the bound Ru(bpy)$_2$(mbpy) isomer. Covalently bound Ru(bpy)$_2$(mbpy) is situated on the protein surface and tilted toward the [2Fe-2S] cluster (Figure 3A).

Fitting a subset of C$^\alpha$ positions of Ru(bpy)$_2$(mbpy)−Adx(1−108) onto Adx(4−108) showed that coupling of the bipyridyl complex did not influence the overall structure of Adx(1−108) (Supporting Information, Figure S1). The backbones of the superimposed area (residues 6−108) of modified Adx(1−108) and Adx(4−108) are very similar with root-mean-square deviation (rmsd) of 0.337 Å. Two Ru(bpy)$_2$(mbpy)−Adx(1−108) complexes and two Adx(4−108) molecules in their asymmetric units were also compared (Figure S1). The rmsd of C$^\alpha$ positions between two Ru(bpy)$_2$(mbpy)−Adx(1−108) was 0.150 Å, lower than that between two Adx(4−108) molecules, 0.428 Å, probably reflecting the lower resolution of the former structure, 1.85 Å.

Two preferential intramolecular electron-transfer pathways were predicted by the program HARLEM for two complexes in the asymmetric unit. Upon light absorption, an electron in the ruthenium complex is formally transferred from the excited metal center to one of the bipyridyl ligands, so that a metal-to-ligand charge-transfer (MLCT) state is formed. From the excited MLCT state, an electron will further be transferred to the Fe2 atom of the iron−sulfur cluster of Adx(1−108) (Figure 3B). The first pathway is operating for the Δ-isomer of Ru(bpy)$_2$(mbpy) bound to molecules A (11.77 Å) and B (11.95 Å) and for the Λ-configuration in molecule A (12.62 Å) (Figure 3B), and the path begins with a through-space jump from the C^{23} or C^{21} atom of the π-system of the bipyridyl ligand to the carbonyl oxygen of Cys92. Then, the path leads over the covalent bonds of Cys92 to the Fe2 atom. The second path (23.71 Å) for the Λ-isomer in molecule B is longer and leads from C^{39} of Ru(bpy)$_2$(mbpy) via the covalent bonds of the Cys95, Ile94, Gln93, and Cys92 residues to the Fe2 atom (Figure 3B).

Redox Potentials. The redox potentials of Adx, Adx(1−108), and Ru(bpy)$_2$(mbpy)−Adx(1−108) were measured as −282 ± 4.5, −302 ± 4.6, and −306 ± 5.2 mV, respectively. Interestingly, the determined Nernst slopes in eq 1 for these proteins are 26 ± 1.1, 31 ± 1.5, and 28 ± 1.8 mV, respectively (Figure 4). These values are close to 30 mV, indicating that apparently two electrons are transferred from the dye to Adx. Measuring the redox potential of P450$_{cam}$ (−312 ± 5.8 mV), which is known as one-electron-acceptor protein, a slope of 66 ± 2.8 mV was determined. This corresponds to ∼60 mV for a one-electron transfer, as expected.

Light-Induced Reduction. Illumination of Adx(1−108) did not affect its stability, as proved by an unchanged absorption spectrum (data not shown). For Ru(bpy)$_2$(mbpy)−Adx(1−108) a 30−40% absorbance decrease at 414 nm has been observed after 45 min of illumination (Figure 5A). Generally, during irradiation a progressive absorbance increase between 487 and 700 nm was detected with an isosbestic point at 487.5 nm (Figure 5A), and it influenced the shape of the difference spectra of Ru(bpy)$_2$(mbpy)−Adx(1−108). In Figure 5B there is a prominent maximum at 500 nm in the difference spectrum of the photoreduced Ru(bpy)$_2$(mbpy)−Adx(1−108), while a minimum is observed for the chemically reduced Adx(1−108). On the other hand, coupled Adx(1−108) does not reveal a positive peak at 550 nm, as is seen for Adx(1−108). Interestingly, upon addition of sodium dithionite to the Ru(bpy)$_2$(mbpy)−Adx(1−108) sample, the same difference spectrum is obtained as for the $Na_2S_2O_4$-reduced Adx(1−108) (data not shown). Because the absolute extent of the reduction is small in the pure photoreduction experiment, the spectral changes of Adx and of the ruthenium complex might compensate each other. This would, however, imply that small spectral changes of the ruthenium complex occur under illumination. Indeed, those changes were observed when the ruthenium complex alone was illuminated. This may also explain why we obtained only 20−25% of the intensity of the initial spectrum after overnight reoxidation of the photoreduced Adx sample.

A linear relationship between ln(1 − α) and t was observed (Figure 5C). After 45 min data deviated from the linearity and were therefore not included in the plot. Observed rates, k_{obs}, are calculated from the slope: (2.0 ± 0.03) × 10^{-5} s^{-1} (0.01 mM), (6.4 ± 0.1) × 10^{-5} s^{-1} (0.05 mM), and (1.8 ± 0.2) × 10^{-4} s^{-1} (0.17 mM), where errors are the standard deviation from the linear fit (Figure 5C). These rates are used to calculate the rates k_{et}, which are 158.3 ± 22.3 s^{-1} (0.01 mM), 483.1 ± 68.6 s^{-1} (0.05 mM), and 1437.5 ± 327.3 s^{-1} (0.17 mM). From the slope of the plot of k_{et} versus the Ru(bpy)$_2$(mbpy)−Adx(1−108) concentrations (Figure 5D) the intermolecular bimolecular rate constant k_{et2} = (7.98 ± 0.04) × 10^6 M^{-1} s^{-1} was obtained. The y intercept of the linear fit at zero concentration of Ru(bpy)$_2$(mbpy)−Adx(1−108) gives the intramolecular monomolecular rate constant k_{et1} of 80.6 ± 3.6 s^{-1}.

EPR Data. In Adx(1−108) as isolated, the iron−sulfur cluster is in the EPR-silent oxidized [2Fe-2S]$^{2+}$ state. In this state the electron spins on both Fe^{III} irons (each S = $^5/_2$) couple antiferromagnetically to a total spin S = 0. In contrast, the reduced form, [2Fe-2S]$^{1+}$, in which the spins of Fe^{III}

Table 2: X-ray Data Collection and Refinement of the $Ru(bpy)_2(mbpy)$−Adx(1−108) Structure

parameter		value
diffraction data[a]	space group	$P2_12_12_1$
	cell constants *a/b/c* (Å)	50.51/56.97/79.08
	resolution (Å)	1.5
	mosaicity (deg)	0.1
	observed/unique reflections	259462/35907
	redundancy	7.2
	completeness (%) (all data/last shell)	95.7/89.6
	R_{sym}[b] (%) (overall/last shell)	5.4/38.5
	$\langle I/\sigma(I)\rangle$ (overall/last shell)	19.1/4.4
asymmetric unit	complexes/atoms	2/2024
	protein, chains/residues/atoms	2/204/1868
	iron−sulfur clusters/atoms	2/8
	water molecules	215
	ruthenium complex, chains/atoms	2/78
average *B* and *R* factors	$Ru(bpy)_2(mbpy)$−Adx(1−108), *A*/*B* (Å^2)	10.61/11.17
	solvent (Å^2)	18.94
	R^c/R_{free}[d]	16.67/19.26
rmsd of refined atoms	bond distances (Å)	0.012
	bond angles (deg)	3.125
Ramachandran plot statistic	residues in most favored regions (%)	93.7
	residues in additionally/generously/disallowed regions (%)	6.3/0/0

[a] Using XDS. [b] $R_{sym} = \sum|I - \langle I\rangle|/\sum|I|$. [c] $R = \sum|F_o - F_c|/\sum|F_o|$. [d] The free *R* factor was calculated using 5% randomly selected reflections.

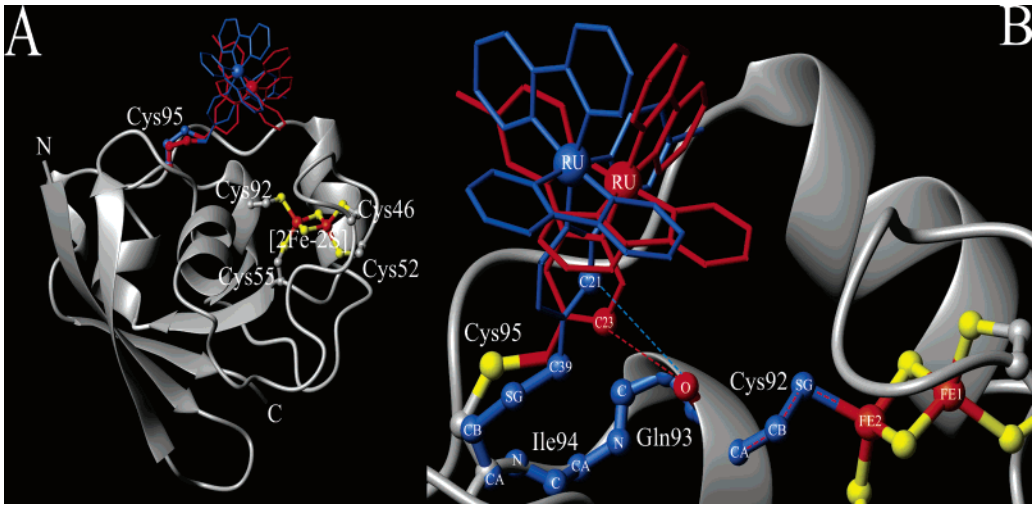

FIGURE 3: Molecular structure of $Ru(bpy)_2(mbpy)$−Adx(1−108). (A) Secondary structure plot of the complex (molecule A). $Ru(bpy)_2$-(mbpy) isomers are in stick representation (Λ, blue, and Δ, red) with the ruthenium atoms as spheres. Cysteine side chains and the [2Fe-2S] cluster are drawn in ball-and-stick representation. (B) Possible electron-transfer pathways calculated by the program HARLEM. Red dotted line: pathway for the Δ-isomer in molecules A and B. Through-space jump from the C^{21} atom of $Ru(bpy)_2(mbpy)$ to the carbonyl O of Cys92 (Λ-isomer in molecule A), marked as a blue dotted line, is followed by further transfer through the covalent bonds of Cys92 (marked also as a red dotted line) as in the Δ-isomer. The path via the protein backbone is shown in blue ball-and-stick representation, starting from C^{39} of $Ru(bpy)_2(mbpy)$. Pictures of the structure were prepared using the program MOLMOL (*49*).

($S = {}^5/_2$) and Fe^{II} ($S = 2$) on both irons couple to a total electron spin $S = {}^1/_2$, is EPR active. Illuminated $Ru(bpy)_3$, Adx(1−108), and a 1:1 mixture of Adx(1−108) plus $Ru(bpy)_3$ showed no EPR signals. The last two results indicate that the $[2Fe\text{-}2S]^{2+}$ cluster stays oxidized after illumination of these samples. In contrast, the typical EPR signal of the reduced $[2Fe\text{-}2S]^{1+}$ cluster was obtained from the chemically and ruthenium-mediated (photochemically) reduced samples of Adx(1−108) and $Ru(bpy)_2(mbpy)$−Adx(1−108), respectively. Two traces, a and b in Figure 6, show that by dithionite reduction of Adx(1−108) two slightly different species of the reduced $[2Fe\text{-}2S]^{1+}$ center were obtained from four samples. The first species exhibits a broader spectrum with *g*-values of $g_{\|} = 2.024(2)$ and $g_{\perp} = 1.938(2)$, which are in excellent agreement with values reported earlier (*33*). In trace b the low-field absorption peak moved to higher field (lower *g*), and the high-field absorption moved to slightly lower field (higher *g*) with corresponding *g*-values of $g_{\|} = 2.012(2)$ and $g_{\perp} = 1.942(2)$, respectively. Although almost all EPR spectra of bovine Adx, which were published in the literature so far, show our first species, the second species has been recently also observed (*34*) for the truncated forms of Adx, Adx(4−108) and Adx(4−114), suggesting a rather different symmetry of the reduced [2Fe-2S] cluster than in the wild-type form. We used always Adx(1−108) only, so that the presence of two slightly different species in one mutant cannot be explained now. However, the [2Fe-2S] cluster is situated near the protein surface, and small structural changes could be induced by different pH values and/or different local dithionite concentrations. The chemically reduced $Ru(bpy)_2(mbpy)$−Adx(1−108) samples (four samples were measured) (trace c in Figure 6) represent a

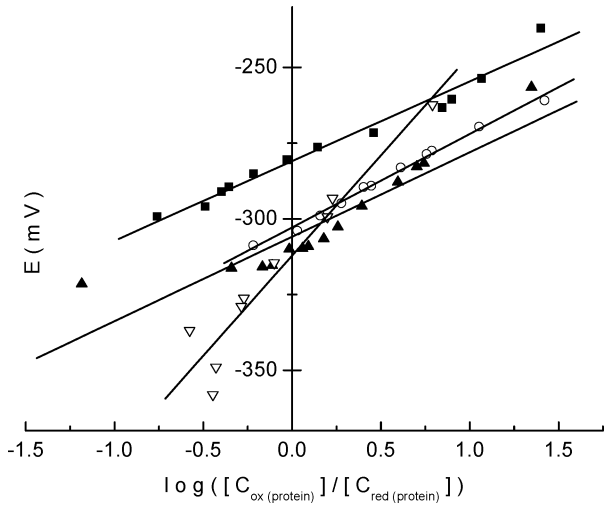

FIGURE 4: Determination of the redox potentials of adrenodoxins and P450$_{cam}$: Adx (■), Adx(1−108) (○), Ru(bpy)$_2$(mbpy)−Adx(1−108) (▲), and P450$_{cam}$ (▽). The *y* intercept of each fitting curve (solid lines) gives the redox potential of a protein. $n_{(protein)}$ for Adx and P450$_{cam}$ could be derived from the slope of every linear fit in the plot. Concentrations of the proteins were in the range between 60 and 70 μM.

superposition of the EPR spectra of the two species above. Trace d in Figure 6 shows the EPR spectrum of the photoreduced [2Fe-2S]$^{1+}$ cluster in the Ru(bpy)$_2$(mbpy)−Adx(1−108) samples (two samples were measured), which are virtually identical with the first species in the chemically reduced unmodified Adx(1−108) sample (Figure 6, trace a).

By spin quantification of the chemically reduced Adx(1−108) samples we have determined that the ratio between the concentration of spins and Adx(1−108) concentration was 1.09 and 1.1 in two independent measurements with an error of ±10%. These results indicate that 100% of the iron−sulfur clusters are in the mixed valence Fe^{II}Fe^{III} state; that means reduced Adx represents the [2Fe-2S]$^{1+}$ state.

DISCUSSION

Many investigations have been already carried out to explore the electron-transfer mechanism in the mitochondrial steroid hydroxylase system of the adrenal cortex which, however, still remains unclear. To probe the shuttle model for the electron transfer, we used an alternative approach, which is based on a light-induced AR-free reduction of bovine adrenodoxin. For this purpose we have covalently modified Adx(1−108) with the ruthenium(II) bipyridyl complex.

Our results reveal four important findings, which concern (i) the successful labeling of Adx with the ruthenium complex and analysis of its 3D structure, (ii) the kinetics of the light-induced reduction of the iron−sulfur cluster of Adx via the labeled ruthenium bipyridyl complex, (iii) comparison of light-induced and chemical reduction of the [2Fe-2S] cluster of Adx by EPR and visible spectroscopy, and (iv) the number of transferred electrons in the safranin T-mediated photoreduction.

Labeling of Adx(*1*−*108*) *with the Ruthenium Complex.* This is the first crystal structure of a ruthenium complex-modified [2Fe-2S] ferredoxin. The bound ruthenium complex protrudes from the Adx(1−108) surface and is oriented toward the [2Fe-2S] cluster (Figure 3A). This position of the complex might affect the cluster microenvironment and, as a consequence, its midpoint potential. The redox potentials of Ru(bpy)$_2$(mbpy)−Adx(1−108) (−306 mV) and Adx(1−108) (−302 mV) are almost identical, indicating an intact iron−sulfur cluster environment. However, differences in the kinetics of cytochrome *c* reduction between Ru(bpy)$_2$(mbpy)-coupled and free Adx(1−108) have been observed, suggesting that labeling might affect intermolecular electron transfer. By molecular modeling and energy minimization for free Adx and cytochrome *c* and the Adx−cytochrome *c* complex, it is proposed that in the complex with the lowest energy the peptide stretches Ile25−Asp31, Cys46−Leu50, Glu68−Glu73, and Cys92−Thr97 of Adx and Val11−Cys17, Lys27−Thr28, and Asn70−Lys86 of cytochrome *c* form the interface (*35*). The Adx peptide stretch Cys92−Thr97 contains the Cys95−Ru(bpy)$_2$(mbpy) modification site. Thus, the slowest kinetics, which was observed for the cytochrome *c* reduction using Ru(bpy)$_2$(mbpy)−Adx(1−108), despite its identical redox potential with Adx(1−108), can be explained by steric hindrance when modified Adx(1−108) and the cytochrome interact.

Kinetics of the Light-Induced Reduction of the Iron−*Sulfur Cluster of Adx.* Ruthenium complex labeling of different heme proteins such as cytochrome b_5 and cytochrome *c* has originally been established by several laboratories to study intramolecular electron-transfer routes and to check the different distance dependence models (*36*, *37*). Our studies show that the electron-transfer rate depends on the concentration of the ruthenium-labeled Adx(1−108), indicating intermolecular transfer taking place ($k_{et2} = \sim 8 \times 10^6$ M^{-1} s^{-1}). The intermolecular electron transfer was also observed in previous studies of ruthenium complex-labeled cytochrome P450$_{cam}$ (*16*). Extrapolation to an Adx concentration of zero gives the intramolecular rate constant, which is found to be ∼81 s^{-1}. Considering the driving force ΔG of ∼0.5 V for the excited state of the ruthenium complex (Ru(II)*) to oxidized Adx(1−108), which was estimated from the redox potentials of ∼−0.8 V (*38*) and ∼−0.3 V for the Ru(II)* and the [2Fe-2S] cluster, respectively, the distances of ∼7−9 Å between two redox groups have been estimated from the Dutton plot (*39*). This distance range is close to the average edge-to-edge distances of 9−10 Å from the ruthenium ligand (C^{23} and C^{21} atom) to Fe2 (Figure 3B), but it is shorter than the HARLEM-determined pathways, 12−13 Å. According to the concept of the Dutton plot (*39*), the electron-transfer rate is determined only by the distance between the redox pair (e.g., in the present work 7−9 Å), with specific electron tunneling pathways being insignificant in biological electron transfer. This is a major difference from the "pathway" (*40*) model in which specific tunneling paths are expected to play a more significant role in biological electron transfer. The obtained distances/paths cannot be compared, despite the small difference between them, because the theoretical model for their determination is different. Nevertheless, if one considers the recently developed (*41*, *42*) "worm" model for determining the electron-transfer pathways, one may reconcile the "straight-line" and pathway models. The worm model roughly assumes a straight line between donor and acceptor, where the paths wind along this line and reflect in that way the specific role of the microenvironment of the protein structure. Thus, on the basis of this assumption the present HARLEM-determined path-

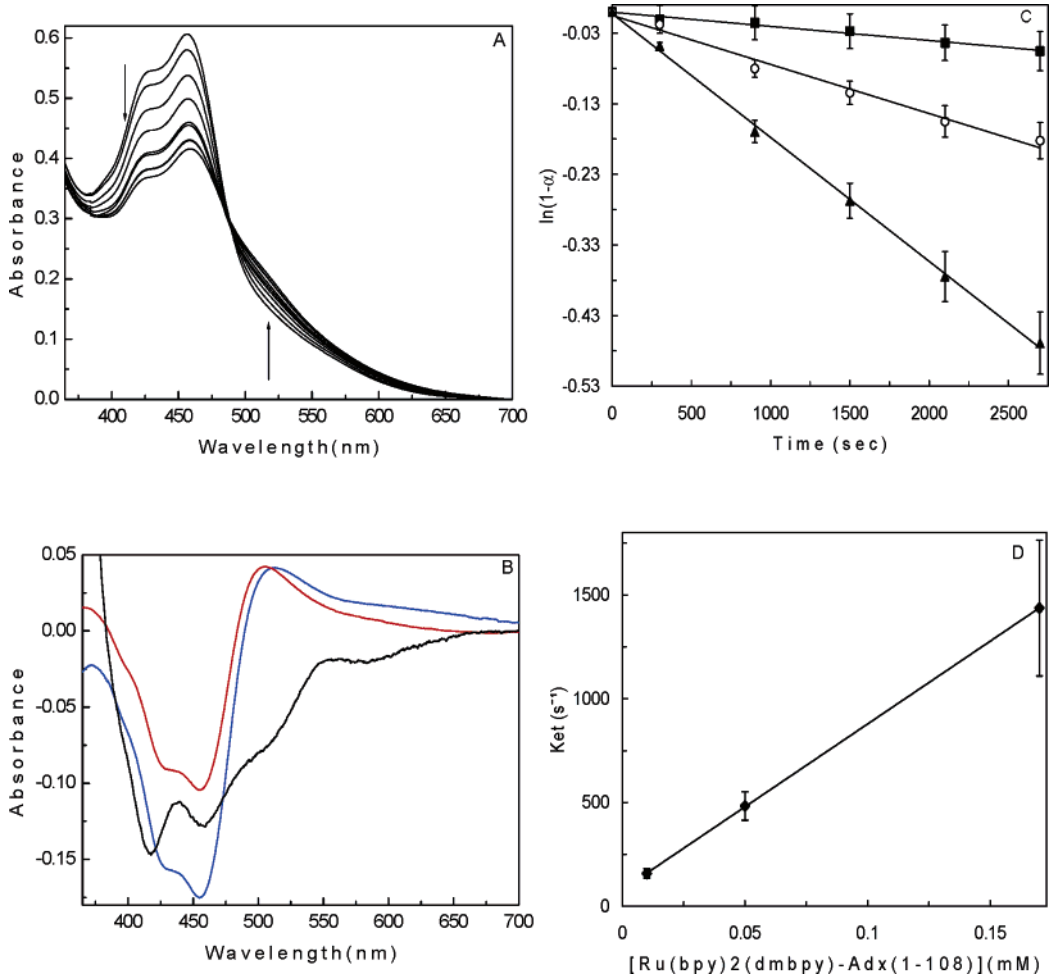

FIGURE 5: Photoreduction of Adx(1−108). (A) Absorption spectra of oxidized and photoreduced (from 15 to 75 min) 1:1 $Ru(bpy)_2$-(mbpy)−Adx(1−108) were obtained under anaerobic conditions. The downward and upward arrows indicate the absorbance decrease at 414 nm and increase between 487 and 700 nm, respectively. (B) Difference spectra of the photoreduced $Ru(bpy)_2$(mbpy)−Adx(1−108) after 15 (red) and 75 min (blue) and chemically reduced Adx(1−108) (black). (C) Formation of photoreduced $Ru(bpy)_2$(mbpy)−Adx(1−108) as a function of the illumination time. Solid lines are linear fits of the function $\ln(1 - \alpha) = -k_{obs}t$ at 0.01 mM (■), 0.05 mM (○), and 0.17 mM (▲) $Ru(bpy)_2$(mbpy)−Adx(1−108) complex, respectively. Error bars correspond to relative errors of the reduced fraction $|\Delta\alpha/\alpha|$ of 50.5% (0.01 mM), 11.8% (0.05 mM), and 7.7% (0.17 mM) at 2700 s. (D) Plot of k_{et} versus $Ru(bpy)_2$(mbpy)−Adx(1−108) concentrations (◆). Error bars correspond to the confidence intervals with the significance level equal to 0.05.

ways (∼12−13 Å) and Dutton distances (∼7−9 Å) are (i) in the distance range for biological electron transfer (*38*) and (ii) could be assigned to the determined intramolecular rate constant.

EPR and Visible Spectra of the (*Photo*)*reduced [2Fe-2S] Cluster of Adrenodoxin.* The EPR spectrum of the chemically reduced Adx samples shows two species [$g_{||} = 2.024(2)$, $g_{\perp} = 1.938(2)$ and $g_{||} = 2.012(2)$, $g_{\perp} = 1.942(2)$] (Figure 6, traces a and b), whose population may depend on solvent conditions and freezing procedures as described elsewhere (*43*). The EPR spectrum of the photoreduced ruthenium complex-coupled Adx does not possess specific new *g*-values, but it shows only one of the two reduced $[2Fe\text{-}2S]^{1+}$ species mentioned above, which seems to be stabilized in this complex. These EPR data show that the attachment of the ruthenium complex does not affect the local geometry of the iron−sulfur cluster. Moreover, it indicates that the photoreduction of Adx via a covalently attached ruthenium complex can be achieved. It is not clear, however, why the chemically reduced ruthenated Adx always showed the presence of two species, which was also observed for the chemically reduced, unmodified Adx samples.

During chemical reduction, the absorption decrease through the entire UV−vis spectrum (260−700 nm) of Adx was monitored. The main features, however, are the appearance of the prominent negative peaks at 414 and 450 nm and, at the later stages of the reduction, of the positive peak at 550 nm. The UV−vis spectrum of the chemically reduced ruthenated Adx(1−108) did not differ from that of the uncoupled, dithionite-reduced protein, but the spectrum of the photoreduced modified ferredoxin shows different features. These differences are clearly visible in the difference spectra of Adx (Figure 5B). However, the insufficient photoreduction level of Adx and possible irreversible spectral changes of the ruthenium complex itself cannot clearly explain the observed spectral differences that arise from applying two reduction techniques.

Number of Transferred Electrons in Safranin T-Mediated Photoreduction. The observed slope of ∼30 mV in the Nernst plot for Adx, Adx(1−108), and $Ru(bpy)_2$(mbpy)−Adx(1−108) indicates that the safranin T-mediated photoreduction leads apparently to the transfer of two electrons to adrenodoxin. The earliest potentiometric titration studies on Adx revealed that the number of accepted electrons per mole of

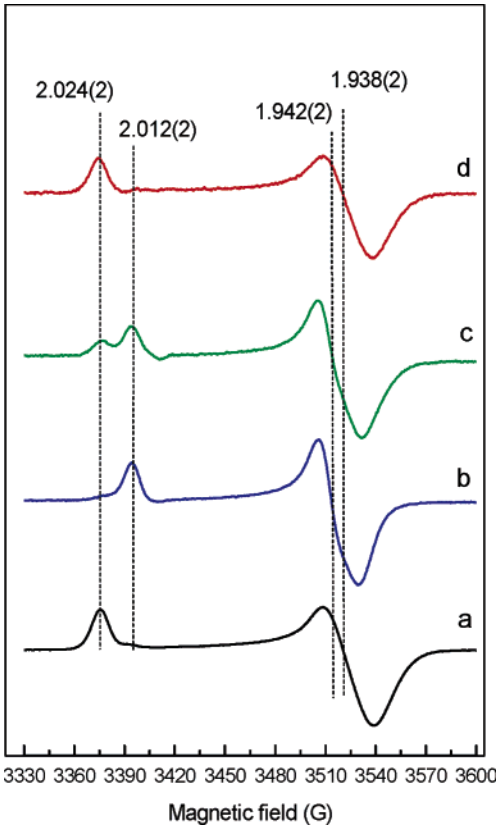

FIGURE 6: EPR spectra of the (photo)reduced [2Fe-2S] cluster of Adx(1−108). Traces a and b are EPR spectra of the chemically reduced iron−sulfur cluster of Adx(1−108). Trace c is the EPR spectrum of the dithionite-reduced cluster of Ru(bpy)$_2$(mbpy)−Adx-(1−108). Trace d is the EPR spectrum of the photoreduced [2Fe-2S] cluster of Ru(bpy)$_2$(mbpy)−Adx(1−108).

the protein, known as a one-electron-carrier protein, is two (*44*). These data are also supported by the anaerobic titration with NADPH in the presence of AR (*45*). In the present work, an artifact or wrong application of the safranin T method is excluded, because for a typical one-electron-acceptor protein, here P450$_{cam}$, a Nernst slope of 66 mV was obtained, as is expected. However, the spin quantification based on the EPR spectra of Adx indicates that just one spin per Adx molecule is localized in the iron−sulfur cluster (Figure 6, trace a), excluding the possibility that the iron−sulfur cluster itself of one Adx molecule accepts and stores both electrons.

The most plausible explanation for this apparent contradiction is that two electrons are tranferred from safranin T to two Adx molecules. These may be present in the monomeric or dimeric state and may simultaneously (two electrons at a time) or sequentially (one electron at a time, as suggested in ref *13*) accept in total two electrons from the dye, i.e., one electron per iron−sulfur cluster of each protein molecule. This model is supported by the fact that oxidized Adx exists both as a monomer and as a dimer (*5*, *46*). Beilke et al. (*8*) have proposed a mechanism of electron transfer via Adx dimers that represents a variant of the shuttle model suggested by Lambeth et al. (*2*). However, only reduced monomeric Adx will be active in transporting electrons to P450$_{scc}$ (*47*), whereas monomeric (*33*, *48*) and perhaps dimeric oxidized protein can inhibit the side-chain cleavage turnover in vivo by binding to P450$_{scc}$.

In this study, we have successfully established the photoreduction of Adx(1−108), which encourages us to further develop this approach to study electron transfer to P450$_{scc}$ via the Ru(bpy)$_2$(mbpy)−Adx(1−108) complex. This may help to finally prove or disprove the shuttle hypothesis of electron transfer by adrenodoxin. The generation of a Ru(bpy)$_2$(mbpy)−Adx(1−108) complex which is chemically cross-linked to P450$_{scc}$ in the previously established orientation (*7*) and capable of transferring electrons to its heme upon photoactivation would demonstrate that higher order complexes involving adrenodoxin reductase are not required for electron transfer in steroid hormone biosynthesis.

ACKNOWLEDGMENT

We thank Dr. Eva-Christina Müller for carrying out mass spectrometry experiments. We also thank Dr. Katja Fälber for collecting the crystallographic data at the SLS. The authors thank Drs. Heinz Welfle and Lubomír Dostál for providing an argon ion laser for photoreduction experiments.

SUPPORTING INFORMATION AVAILABLE

One figure showing distance differences between C$^{\alpha}$ atom pairs. This material is available free of charge via the Internet at http://pubs.acs.org.

REFERENCES

1. Hanukoglu, I., Privalle, C. T., and Jefcoate, C. R. (1981) Mechanisms of ionic activation of adrenal mitochondrial cytochromes P-450$_{scc}$ and P-45011β, *J. Biol. Chem. 256*, 4329−4335.
2. Lambeth, J. D., Seybert, D. W., Lancaster, J. R., Salerno, J. C., and Kamin, H. (1982) Steroidogenic electron transport in adrenal cortex mitochondria, *Mol. Cell. Biochem. 45*, 13−31.
3. Kido, T., and Kimura, T. (1979) The formation of binary and ternary complexes of cytochrome P-450$_{scc}$ with adrenodoxin and adrenodoxin reductase-adrenodoxin complex. The implication in ACTH function, *J. Biol. Chem. 254*, 11806−11815.
4. Hara, T., and Takeshima, M. (1994) Conclusive evidence of a quartery cluster model for cholesterol side-chain cleavage reaction catalyzed by cytochrome P450$_{scc}$, in *Cytochrome P450. 8th International* Conference (Lechner, M. C., Ed.) pp 417−420, John Libbey Eurotext, Paris, France.
5. Müller, A., Müller, J. J., Muller, Y. A., Uhlmann, H., Bernhardt, R., and Heinemann, U. (1998) New aspects of electron transfer revealed by the crystal structure of a truncated bovine adrenodoxin, Adx(4−108), *Structure 6*, 269−280.
6. Müller, J. J., Lapko, A., Bourenkov, G., Ruckpaul, K., and Heinemann, U. (2001) Adrenodoxin reductase-adrenodoxin complex structure suggests electron-transfer path in steroid biosynthesis, *J. Biol. Chem. 276*, 2786−2789.
7. Müller, E.-Ch., Lapko, A., Otto, A., Müller, J. J., Ruckpaul, K., and Heinemann, U. (2001) Covalently cross-linked complex of bovine adrenodoxin with adrenodoxin reductase and cytochrome P450$_{scc}$. Mass spectrometry and Edman degradation of complexes of the steroidogenic hydroxylase system, *Eur. J. Biochem. 268*, 1837−1843.
8. Beilke, D., Weiss, R., Lohr, F., Pristovsek, P., Hannemann, F., Bernhardt, R., and Rüterjans, H. (2002) A new electron transport mechanism in mitochondrial steroid hydroxylase systems based on structural changes upon the reduction of adrenodoxin, *Biochemistry 41*, 7969−7978.
9. Uhlmann, H., Beckert, V., Schwarz, D., and Bernhardt, R. (1992) Expression of bovine adrenodoxin in *E. coli* and site-directed mutagenesis of /2 FE- -2S/ cluster ligands, *Biochem. Biophys. Res. Commun. 188*, 1131−1138.
10. Studier, F. W. (1991) Use of bacteriophage T7 lysozyme to improve an inducible T7 expression system, *J. Mol. Biol. 219*, 37−44.
11. Lapko, A., Müller, A., Heese, O., Ruckpaul, K., and Heinemann, U. (1997) Preparation and crystallization of a cross-linked complex

of bovine adrenodoxin and adrenodoxin reductase, *Proteins: Struct., Funct., Genet. 28*, 289−292.
12. Chashchin, V. L., Vasilevsky, V. I., Shkumatov, V. M., and Akhrem, A. A. (1984) The domain structure of the cholesterol side-chain cleavage cytochrome P-450 from bovine adrenocortical mitochondria, *Biochim. Biophys. Acta 787*, 27−38.
13. Huang, J. J., and Kimura, T. (1973) Adrenal steroid hydroxylases. Oxidation−reduction properties of adrenal iron−sulfur protein (adrenodoxin), *Biochemistry 12*, 406−409.
14. Chu, J. W., and Kimura, T. (1973) Studies on adrenal steroid hydroxylases. Molecular and catalytic properties of adrenodoxin reductase (a flavoprotein), *J. Biol. Chem. 248*, 2089−2094.
15. Omura, T., and Sato, R. (1964) The carbon monoxide-binding pigment of liver microsomes. I. Evidence for its hemoprotein nature, *J. Biol. Chem. 239*, 2370−2378.
16. Contzen, J., Kostka, S., Kraft, R., and Jung, C. (2002) Intermolecular electron transfer in cytochrome $P450_{cam}$ covalently bound with tris(2,2′-bipyridyl)ruthenium(II): structural changes detected by FTIR spectroscopy, *J. Inorg. Biochem. 91*, 607−617.
17. Sligar, S. G., and Gunsalus, I. C. (1976) A thermodynamic model of regulation: modulation of redox equilibria in camphor monoxygenase, *Proc. Natl. Acad. Sci. U.S.A. 73*, 1078−1082.
18. Stiehler, R. D., Chen, T.-T., and Mansfield Clark, W. (1933) Studies on oxidation−reduction. XVIII. Simple safranines, *J. Am. Chem. Soc. 55*, 891−907.
19. Schwarz, D., Richter, W., Kruger, V., Chernogolov, A., Usanov, S., and Stier, A. (1994) Direct visualization of a cardiolipin-dependent cytochrome $P450_{scc}$-induced vesicle aggregation, *J. Struct. Biol. 113*, 207−215.
20. Keller, P., Moradpour, A., Amouyal, E., and Kagan, H. B. (1980) Hydrogen-production by visible-light using viologen-dye mediated redox cycles, *Nouv. J. Chim. 4*, 377−384.
21. Geren, L., Hahm, S., Durham, F., and Millet, F. (1991) Photoinduced electron transfer between cytochrome *c* peroxidase and yeast cytochrome *c* labeled at Cys102 with (4-bromomethyl-4′-methylbipyridine)[bis(bipyridine)]ruthenium^{2+}, *Biochemistry 30*, 9450−9457.
22. Durham, D., Pan, L. P., Long, J. E., and Millet, F. (1989) Photoinduced electron-transfer kinetics of singly labeled ruthenium bis(bipyridine) dicarboxybipyridine cytochrome *c* derivatives, *Biochemistry 28*, 8659−8665.
23. Shimada, H., Nagano, S., Ariga, Y., Unno, M., Egawa, T., Hishiki, T., Ishimura, Y., Masuya, F., Obata, T., and Hori, H. (1999) Putidaredoxin-cytochrome $P450_{cam}$ interaction. Spin state of the heme iron modulates putidaredoxin structure, *J. Biol. Chem. 274*, 9363−9369.
24. Watari, H., and Kimura, T. (1966) Study of the adrenal non-heme iron protein (adrenodoxin) by electron spin resonance, *Biochem. Biophys. Res. Commun. 24*, 106−112.
25. Kabsch, W. (2001) XDS in *International Tables for Crystallography, Volume F. Crystallography of Biological Macromolecules* (Rossmann, M. G., and Arnold, E., Eds.) Chapter 25.2.9, Kluwer Academic Publishers, Dordrecht.
26. Navaza, J. (1994) *AMoRe*: an automated package for molecular replacement, *Acta Crystallogr. A50*, 157−163.
27. Murshudov, G. N., Vagin, A. A., and Dodson, E. J. (1997) Refinement of macromolecular structures by the maximum-likelihood method, *Acta Crystallogr. D53*, 240−255.
28. Dunn, A. R., Dmochowski, I. J., Bilwes, A. M., Gray, H. B., and Crane, B. R. (2001) Probing the open state of cytochrome $P450_{cam}$ with ruthenium-linker substrates, *Proc. Natl. Acad. Sci. U.S.A. 98*, 12420−12425.
29. Jones, T. A., Zhou, J.-Y., Cowan, S. W., and Kjeldgaard, M. (1991) Improved methods for building protein models in electron density maps and the location of errors in these models, *Acta Crystallogr. A47*, 110−119.
30. Szoke, A. (1993). Holographic methods in X-ray crystallography. II. Detailed theory and connection to other methods of crystallography, *Acta Crystallogr. A49*, 853−866.
31. Curry, W. B., Grabe, M. D., Kurnikov, I. V., Skourtis, S. S., Beratan, D. N., Regan, J. J., Aquino, A. J., Beroza, P., and Onuchic, J. N. (1995) Pathways, pathway tubes, pathway docking and propagators in electron transfer proteins, *J. Bioenerg. Biomembr. 27*, 285−293.
32. Kabsch, W. (1976) A solution for the best rotation to relate two sets of vectors, *Acta Crystallogr. A32*, 922−923.
33. Tuckey, R. C., McKinley, A. J., and Headlam, M. J. (2001) Oxidized adrenodoxin acts as a competitive inhibitor of cytochrome $P450_{scc}$ in mitochondria from the human placenta, *Eur. J. Biochem. 268*, 2338−2343.
34. Uhlmann, H., Kraft, R., and Bernhardt, R. (1994) C-terminal region of adrenodoxin affects its structural integrity and determines differences in its electron-transfer function to cytochrome P-450, *J. Biol. Chem. 269*, 22567−22564.
35. Müller, J. J., Lapko, A., Ruckpaul, K., and Heinemann, U. (2003) Modeling of electrostatic recognition processes in the mammalian mitochondrial steroid hydroxylase system, *Biophys. Chem. 100*, 281−292.
36. Scott, J. R., Willie, A., McLean, M., Stayton, P. S., Sligar, S. G., Durham, B., and Millett, F. (1993) Intramolecular electron transfer in cytochrome b_5 labelled with ruthenium(II) polypyridine complexes: rate measurements in the Marcus inverted region, *J. Am. Chem. Soc. 115*, 6820−6824.
37. Sun, J., Wishart, J. F., van Eldik, R., Shalders, R. D., and Swaddle, T. W. (1995) Pressure tuning voltammetry. Reaction volumes for electron transfer in cytochrome *c* and ruthenium-modified cytochromes *c*, *J. Am. Chem. Soc. 117*, 2600−2605.
38. Juris, A., Balzani, V., Barigelletti, F., Campagna, S., Belser, P., and Vonzelewsky, A. (1988) Ru(II) polypyridine complexes: photophysics, photochemistry, electrochemistry, and chemiluminescence, *Coord. Chem. Rev. 84*, 85−277.
39. Page, C. C., Moser, C. C., Chen, X., and Dutton, L. (1999) Natural engineering principles of electron tunnelling in biological oxidation−reduction, *Nature 402*, 47−52.
40. Onuchic, J. N., Beratan, D. N., Winkler, J. R., and Gray, H. B. (1992) Pathway analysis of protein electron-transfer reactions, *Annu. Rev. Biophys. Biomol. Struct. 21*, 349−377.
41. Kawatsu, T., Kakitani, T., and Yamato, T. (2000) A novel method for determining the electron tunnelling pathways in protein, *Inorg. Chim. Acta 300−302*, 862−868.
42. Kawatsu, T., Kakitani, T., and Yamato, T. (2001) Worm model for electron tunnelling in proteins: consolidation of the pathway model and the Dutton plot, *J. Phys. Chem. 105*, 4424−4435.
43. Mukai, K., Kimura, T., Helbert, J., and Kevan, L. (1973) Environment of the iron−sulfur chromophore in adrenodoxin studied by EPR and ENDOR spectroscopy, *Biochim. Biophys. Acta 295*, 49−56.
44. Kimura, T., and Suzuki, K. (1967) Components of the electron transport system in adrenal steroid hydroxylase. Isolation and properties of non-heme iron protein (adrenodoxin), *J. Biol. Chem. 242*, 485−491.
45. Kimura, T., and Suzuki, K. (1965) Enzymatic reduction of non-heme iron protein (adrenodoxin) by reduced nicotinamide adenine dinucleotide phosphate, *Biochem. Biophys. Res. Commun. 20*, 373−379.
46. Pikuleva, I. A., Tesh, K., Waterman, M. R., and Kim, Y. (2000) The tertiary structure of full-length bovine adrenodoxin suggests functional dimers, *Arch. Biochem. Biophys. 373*, 44−55.
47. Tsubaki, M., Hiwatashi, A., and Ichikawa, Y. (1989) Conformational change of the heme moiety of ferrous cytochrome $P\text{-}450_{scc}$-phenyl isocyanide complex upon binding of reduced adrenodoxin, *Biochemistry 28*, 9777−9784.
48. Lambeth, J. D., and Pember, S. O. (1983) Cytochrome P-450scc-adrenodoxin complex. Reduction properties of the substrate-associated cytochrome and relation of the reduction states of heme and iron−sulfur centers to association of the proteins, *J. Biol. Chem. 258*, 5596−5602.
49. Koradi, R., Billeter, M., and Wüthrich, K. (1996) MOLMOL: a program for display and analysis of macromolecular structures, *J. Mol. Graphics 14*, 51−55.

BI0510330